

## PHYSICS

## Ninety percent circular polarization detected in a repeating fast radio burst

J. C. Jiang<sup>1</sup>, J. W. Xu<sup>2,3</sup>, J. R. Niu<sup>1</sup>, K. J. Lee<sup>2,1,4,\*</sup>, W. W. Zhu<sup>1,\*</sup>, B. Zhang<sup>5,6,\*</sup>, Y. Qu<sup>5,6</sup>, H. Xu<sup>1</sup>, D. J. Zhou<sup>1</sup>, S. S. Cao<sup>2</sup>, W. Y. Wang<sup>7</sup>, B. J. Wang<sup>1</sup>, S. Cao<sup>8</sup>, Y. K. Zhang<sup>1</sup>, C. F. Zhang<sup>1</sup>, H. Q. Gan<sup>1</sup>, J. L. Han<sup>1</sup>, L. F. Hao<sup>8</sup>, Y. X. Huang<sup>8</sup>, P. Jiang<sup>1</sup>, D. Z. Li<sup>9</sup>, H. Li<sup>1</sup>, Y. Li<sup>10</sup>, Z. X. Li<sup>8</sup>, R. Luo<sup>11</sup>, Y. P. Men<sup>12</sup>, L. Qian<sup>1</sup>, J. H. Sun<sup>1</sup>, L. Wang<sup>3</sup>, Y. H. Xu<sup>8</sup>, R. X. Xu<sup>2,14</sup>, Y. P. Yang<sup>13</sup>, R. Yao<sup>1</sup>, Y. L. Yue<sup>1</sup>, D. J. Yu<sup>1</sup>, J. P. Yuan<sup>15</sup> and Y. Zhu<sup>1</sup>

## ABSTRACT

Fast radio bursts (FRBs) are extra-galactic sources with unknown physical mechanisms. They emit millisecond-duration radio pulses with isotropic equivalent energy of  $10^{36} \sim 10^{41}$  ergs. This corresponds to a brightness temperature of FRB emission typically reaching the level of  $10^{36}$  K, but can be as high as above  $10^{40}$  K for sub-microsecond timescale structures, suggesting the presence of underlying coherent relativistic radiation mechanisms. Polarization carries the key information to understand the physical origin of FRBs, with linear polarization usually tracing the geometric configuration of magnetic fields and circular polarization probing both intrinsic radiation mechanisms and propagation effects. Here we show that the repeating source FRB 20201124A emits  $90.9 \pm 1.1\%$  circularly polarized radio pulses. Such a high degree of circular polarization was unexpected in theory and unprecedented in observation in the case of FRBs, since such a high degree of circular polarization was only common among Solar or Jovian radio activities, attributed to the sub-relativistic electrons. We note that there is no obvious correlation between the degree of circular polarization and burst fluence. Besides the high degree of circular polarization, we also detected rapid swing and orthogonal jump in the position angle of linear polarization. The detection of the high degree circular polarization in FRB 20201124A, together with its linear polarization properties that show orthogonal modes, place strong constraints on FRB physical mechanisms, calling for an interplay between magnetospheric radiation and propagation effects in shaping the observed FRB radiation.

**Keywords:** radio astronomy, fast radio burst, polarization

## INTRODUCTION

Within the framework of the magnetar engine as suggested by the detection of the Galactic FRB 20200428D [1,2], two major types of models have been proposed [3], the far-away, gamma-ray burst (GRB)-like models that invokes synchrotron maser in highly magnetized, relativistic shocks [4,5] and the closer-in, pulsar-like models that invokes radio emission from magnetospheres [6–11]. Previous observations already provided crucial polarization properties of FRBs, including linear polarization angle swings [12–19], and oscillations between linear and cir-

cular polarizations [14].

Moderate levels of circular polarization from 5% to 57% had been reported for FRBs without observed repetition, i.e. for FRB 20110523A [20], 20140514A [21], 20160102A [22], 20180309A [23], 20180311A [23], 20180714A [23], 20180924B [24], 20181112A [25,26], 20190102C [24], 20190608B [24], 20190611B [24], and 20191219F [27]. Repeating FRBs mostly show low level of circular polarization (a few percent) and only a few of them emit significant circular polarization for a small fraction of bursts, i.e. FRB 20190520B [28] (42%) FRB 20201124A

<sup>1</sup>National Astronomical Observatories, CAS, Beijing 100101, China;

<sup>2</sup>Department of Astronomy, Peking University, Beijing 100871, China;

<sup>3</sup>Kavli Institute for Astronomy and Astrophysics, Peking University, Beijing 100871, China;

<sup>4</sup>Beijing Laser Acceleration Innovation Center, Beijing 101400, China;

<sup>5</sup>Nevada Center for Astrophysics, University of Nevada, Las Vegas NV 89154, USA;

<sup>6</sup>Department of Physics and Astronomy, University of Nevada, Las Vegas NV 89154, USA;

<sup>7</sup>School of Astronomy and Space Science, University of Chinese Academy of Sciences, Beijing 100049, China;

<sup>8</sup>Yunnan Observatories, CAS, Kunming 650216, China;

<sup>9</sup>Department of Astrophysical Sciences, Princeton University, Princeton NJ 08544, USA;

<sup>10</sup>Purple Mountain Observatory, CAS, Nanjing 210008, China;

<sup>11</sup>School of Physics and Electronic Engineering, Guangzhou University, Guangzhou 510006, China;

<sup>12</sup>Max-Planck institut für Radioastronomie, Bonn 53121, Germany;

<sup>13</sup>South-Western Institute For Astronomy Research, Yunnan University, Kunming 650504, China;

<sup>14</sup>State Key Laboratory of Nuclear Physics and Technology, Peking University, Beijing 100871, China;

<sup>15</sup>Xinjiang Astronomical Observatory, CAS, Urumqi 830011, China

\*Corresponding authors.

Email: [kilee@pku.edu.cn](mailto:kilee@pku.edu.cn)

© The Author(s), 2024. Published by Oxford University Press on behalf of China Science Publishing & Media Ltd. This is an Open Access article distributed under the terms of the Creative Commons Attribution License (<http://creativecommons.org/licenses/by/4.0/>), which permits unrestricted reuse, distribution, and reproduction in any medium, provided the original work is properly cited.

Received: XX XX Year;

Revised: XX XX Year;

Accepted: XX XX Year

[14–18] ( $\sim 75\%$ ), FRB 20121102A [29] (64%), and FRB 20220912A [19,30,31] (70%). Among the sources, the FRB 20201124A is an active repeating FRB source with event rate as high as  $542 \text{ hr}^{-1}$  during its active window [14,17,32–34]. Previous observations have detected 1863 bursts from the source using the Five-hundred-meter Aperture Spherical radio Telescope (FAST) in the L-band (centered at 1.25 GHz) during one of its active periods between March and May, 2021 [14]. It entered a new period of activity on September 21, 2021 according to the alert from the Canadian Hydrogen Intensity Mapping Experiment (CHIME) [35]. Following the detections, we scheduled daily FAST observations to monitor the source between September 25 and October 2, 2021 [17,32–34]. Here we report the detection of highly circularly polarized (with the degree of circular polarization  $\geq 90.9 \pm 1.1\%$ ) radio pulses from FRB 20201124A with FAST. The observation serves as a touchstone for FRB radiation models and suggests extreme conditions for the generation and propagation of FRBs in the nearby environment.

## RESULTS

In the new active window, we detected a group of highly circularly polarized bursts from FRB 20201124A and found the evidence of orthogonal polarization modes, i.e. dual linear polarization modes with orthogonal directions. In a total of 536 bursts with signal-to-noise ratio (S/N) higher than 50 out of more than 800 bursts above the detection threshold  $S/N \geq 7$ , we detected a group of 15 bursts with average degrees of circular polarization  $\Pi_V \equiv |V|/I > 50\%$  and 106 bursts with  $\Pi_V \geq 20\%$ . A selected sample of bursts with significant circular polarization is shown in Fig. 1, while other bursts with peak  $\Pi_V > 50\%$  are shown in Figure S4-7 and their properties are summarized in Table S1.

As shown in Fig. 1, the time-averaged  $\Pi_V$  of Bursts 266, 299 and 521 were  $(-71.1 \pm 0.4)\%$ ,  $(73.5 \pm 0.7)\%$  and  $(-90.9 \pm 1.1)\%$ , respectively, while the time-resolved  $\Pi_V$  could be even higher. The degree of circular polarization of Burst 521 is larger than any FRB bursts previously reported. The two bursts have opposite handedness of circular polarization. In Burst 299, the circular polarization is left hand, while the right hand mode dominates Burst 521. The burst profile of both bursts showed double-peak structure in total intensity  $I$ , linear polarization intensity  $L$ , and circular polarization intensity  $V$ . The linear polarization position angle (PA) remained constant

across the two peaks.

In Fig. 1, we also show the two adjacent bursts (Bursts 298 and 300) of Burst 299, as they are only separated by a few tens of milliseconds from Burst 299. Despite the temporal proximity, these three bursts show rather different polarization properties. The degree of circular polarization of Burst 298 is similar to that of Burst 299. However, the PA changed abruptly by approximately  $60^\circ$ . Bursts 299 and 300 had the same PA, while the degree of circular polarization drops from  $73.5\%$  to  $12.2 \pm 1.9\%$  within less than 20 ms. In the spectral domain, the degree of linear polarization ( $\Pi_L \equiv L/I$ ) and  $\Pi_V$  remained almost constant across the observed bandwidth of bursts (Figure S1), i.e. there is no obvious polarization evolution or oscillations [14] from 1.0 GHz to 1.4 GHz.

Despite the similarities in Bursts 299 and 521, the circular polarization phenomena for FRB 20201124A are of a great diversity. From the morphology perspective, not all high degree of circular polarization is associated with the double-peak pulse structure like Bursts 299 and 521. As an example, Burst 123 in Fig. 1 with  $\Pi_V = -52\%$  has a single peak pulse. One can also note clear variations of  $\Pi_V$  across the phase in Burst 123, opposite to the case of Bursts 299 and 521. For the bursts with lower degrees of circular polarization, we have found single-peak pulses with circular polarization sign reversal (Burst 269), which is shown in Fig. 1. We also identified abrupt  $90^\circ$  jumps in PA of linear polarization. An example (Burst 738) is shown in Fig. 1, where a  $90^\circ$  jump occurs at 30 ms. One can notice that the degree of circular polarization peaked at the time of the  $90^\circ$  PA jump.

## DISCUSSION

The substantially high circular polarization degree observed in a few bursts provides valuable insights into unraveling the coherent radiation mechanism of FRBs. Our immediate conclusion is that the far-way GRB-like models, which invoke maser-type emission from relativistic shocks outside the magnetosphere [4,5], are not supported by the data. In general, circular polarization of emission can be generated either from intrinsic radiation mechanisms or through propagation effects. Both mechanisms fail to accommodate the data for GRB-like models. First, it has been shown [11] that the 90% circular polarization from a bright burst cannot be generated from the intrinsic synchrotron maser (the relativistic version of cyclotron maser [36]) model. This is because the

synchrotron maser model requires ordered magnetic fields in the shock plane, and the observed radiation predominately carries high linear polarization. Circular polarization is possible with off-beam viewing geometry, but these high  $\Pi_v$  bursts are expected to have much lower fluxes than other bursts, inconsistent with the bright high  $\Pi_v$  bursts we detected. GRB-like models are also disfavored due to rapid swings of PA curves, which has been observed in the emission from other repeaters FRB 20180301A [13] and FRB 20220912A [19].

Our results also challenge the out-of-magnetosphere propagation models for the circular polarization. Propagation models might plausibly incorporate Faraday conversion and synchrotron or cyclotron absorption to generate a high degree of circular polarization [11,14,37–39]. However, these models encounter difficulties in elucidating the dynamics observed in the three successive bursts within 30 milliseconds, Bursts 298, 299, and 300, as depicted in Fig. 1. As out-of-magnetosphere propagation effects will simultaneously affect both linear and circular polarizations for all pulses, intricate conditions have to be satisfied, such that 1) the PA changed significantly while  $\Pi_v$  and  $\Pi_L$  remained nearly constant (Bursts 298 and 299), and 2)  $\Pi_v$  changed while PA being constant (Bursts 299 and 300). It is essentially impossible for an external plasma to make such abrupt changes within a timescale of 30 milliseconds. Furthermore, Bursts 521 and 123 exhibited a frequency-independent degrees of circular or linear polarization, rendering the models centered solely on propagation effects increasingly difficult, because both Faraday conversion and synchrotron/cyclotron absorption processes will typically exhibit frequency dependent polarization. Furthermore, the absorption-related models require a non-negligible value of the optical depth to produce high circular polarization [11,40], and thus predict a lower flux for high  $\Pi_v$  bursts. As a result, these mechanisms also suffer from the flux problem similar to the one the synchrotron maser emission model faces.

The data are more consistent with pulsar-like models that invoke emission inside a magnetar magnetosphere. For the intrinsic radiation models, two widely discussed magnetospheric mechanisms to explain the high brightness temperatures of FRB radio emission [41] involve either curvature radiation [6–8] or inverse Compton scattering (ICS) mechanisms [10,42,43] of particle bunches. Regarding curvature radiation

[9], circular polarization can be generated, when the observer’s line of sight slightly deviates from the center of radiation beam, resulting in seeing the circular motion of electrons and detecting the corresponding circular polarization. For ICS, the scattered emission by a single particle is linearly polarized, but circular polarization can be generated as a consequence of emission from a bunch with certain geometry. In particular, when the line of sight mis-aligns with the direction of the ICS electron bunch, circular polarization could be detected, as different phases are superposed to the scattered radiation induced by the different parts of the bunch [11]. A high circular polarization degree can be generated slightly off-axis, even when the line of sight is still within the  $1/\gamma$  relativistic beaming cone of the relativistic bunch ( $\gamma$  being the Lorentz factor of the bunch).

We noted the sign reversal of  $\Pi_v$  with an example showing in Burst 269. This phenomenon closely aligns with the predictions of the both curvature radiation and ICS models, which predict the reversal of the sign of circular polarization when the line of sight sweeps across the meridian plane of the electron’s trajectory, and hence, provides a strong support to the magnetospheric origin of FRB emission. In the mean time, our observations also provide constraints on these models. In general, since circular polarization is observed off-beam in both models, one should generally expect a systematically fainter population for the high  $\Pi_v$  bursts. We compared the fluence distributions of bursts with  $\Pi_v \geq 50\%$  and  $\Pi_v \leq 50\%$  using the two-sample Kolmogorov-Smirnov test and could not find evidence that the bursts with  $\Pi_v \geq 50\%$  are systematically fainter (see Supplementary materials). Our simulations showed that one would detect the difference at a confidence level higher than 95%, if the energies of  $\Pi_v \geq 50\%$  bursts are reduced to 65% of the observed values. Theories for FRB radiation need to address whether the models can reproduce the independence between the distributions of circular polarization degree and burst fluence. Another interesting constraint comes from the nearly constant degree of circular polarization as observed in Burst 521, which requires that the line of sight should maintain a nearly constant angle relative to the center of radiation beam in the entire burst. This is possible for the ICS mechanism which predicts a similar  $\Pi_v$  in a wide range of azimuthal angle with respect to a bunch [11] and may suggest a non-steady plasma flow along the magnetic field lines [9] or a very special geometric configuration of magnetic field, electron velocity, and line

of sight for the curvature radiation model.

Our results may be also accommodated for wave propagation within the magnetosphere. A possible explanation to the differences between Bursts 298, 299 and 300 is that the three bursts originate from different depths in a magnetosphere, and propagate different distances before escaping. Since circular polarization may be generated during wave propagation, Burst 300 with the least amount of circular polarization might be least affected by propagation effects among the three bursts. Another hint of magnetospheric propagation is that Bursts 738 shows a sudden  $90^\circ$  jump in the linear polarization position angle (approximately at  $\sim 30$  ms in Fig. 1). Similar features have been widely detected in pulsars, mostly in the averaged pulse profiles [44], but sometimes in single pulses as well [45]. Such orthogonal jumps can be attributed to the superposition of two linearly polarized wave modes (O-mode and X-mode) either incoherently [44] or coherently [46]. For our case, the observed PA jump occurs within a single burst, and degree of circular polarization forms a peak at the PA-jump epoch accompanied with a nearly full depolarization of linear polarization. These behaviors suggest a possible coherent superposition between the two linear polarization modes. It is more plausible that the two modes were excited by the same group of electrons, and the propagation effects, such as birefringence, within magnetosphere induced the  $90^\circ$  PA jump. Our results indicate that the propagation effects need also maintain a  $90^\circ$  phase difference between the two modes to ensure that linear polarization is depolarized and circular polarization dominates at the epoch of PA jump. The multi-path propagation effect [47] can cancel linear polarization and keep circular polarization components, but it is unexpected that the  $\Pi_v$  peaks at the PA jump.

FRB 20201124A belongs to a unique type of source. In Fig. 2, we summarized astrophysical radio sources known so far to exhibit significant circular polarization. One can see that FRB 20201124A stands out in the parameter space of high  $\Pi_v$  and high luminosity. The other examples with high degree of circular polarization include Type I and Type IV solar storms, as well as solar storm continua and microwave spikes, which can reach the degree of circular polarization similar to that of Burst 521. Additionally, the magnetosphere of Jupiter have been observed to generate highly circularly polarized radio emission. Unlike in the case of FRBs, these sources of high circular polarization are pow-

ered by sub-relativistic plasma. The circular polarization are mainly generated from cyclotron radiation. In contrast, the high luminosity and high degree of circular polarization in the case of FRBs demand relativistic plasma emission in a new parameter regime, which differs from all known radio sources known in the past, suggesting extreme conditions for FRB generation and propagation.

In summary, the extreme and diverse polarization properties of FRB 20201124A provide constraints on the physical mechanisms generating the FRB radiation. Although a comparable degree of circular polarization has been observed in solar and Jovian radio emissions, their non-relativistic nature limits the applicability to FRB models. GRB-like models and out-of-magnetosphere propagation models are disfavored for the following reasons: 1) the models cannot account for rapid polarization changes as seen in bursts 298, 299, and 300; 2) the frequency independence of  $\Pi_v$  as observed in bursts 123 and 521 cannot be interpreted by only invoking Faraday conversion and synchrotron/cyclotron absorption, and 3) no strong correlation between flux and circular polarization is detected. In contrast, pulsar-like models and magnetospheric propagation models are more plausible, even though some fine-tuning of these models may be necessary. Among the known radio burst/pulse sources, the high degree of circular polarization, combined with the high brightness temperature, make FRB radiation processes even more mysterious.

## METHODS

The FAST intensively monitor the FRB 20201124A between September 25 and October 17, 2021 [17,32–34]. The L-band receiver covers radio frequency between 1 and 1.5 GHz, divided into 4096 channels. The original time resolution is  $49.152 \mu\text{s}/\text{sample}$ . We used software package *TransientX* [48] to search for bursts in the data, and detected more than 500 bursts with  $S/N > 50$  between September 25 and 27, 2021. More details about observation and burst detection can be found in Section S1 within the Supplementary Data.

The signal from the noise diode was injected to the receiver as the linearly polarized calibrator. The polarimetric calibration was performed using PSRCHIVE [49]. Then, the rotation measure (RM) is measured by fitting the oscillation of Stokes  $Q$  and  $U$ . In this article we follow the PSR/IEEE convention on the definition of Stokes parameters [50]. Our final results shown above



include both the corrections of feed polarization response and Faraday rotation effect. The more details about polarimetry can be found in Section S2 and S3 in the online Supplementary materials.

### Data availability

Raw data are archived and available from the FAST data center, <http://fast.bao.ac.cn>. Owing to the large data volume, we encourage contacting the corresponding author and FAST data center for the data transferring. The directly related data that support the findings of this study can be found at the PSRPKU website, <https://psr.pku.edu.cn/index.php/publications/frb20201124a/>.

CHIME/FRB Public Database can be found at <https://www.chime-frb.ca/repeaters/FRB20201124A>.

### Code availability

PSRCHIVE (<http://psrchive.sourceforge.net>)

TRANSIENTX (<https://github.com/ypmen/TransientX>)

BEAR (<https://psr.pku.edu.cn/index.php/publications/frb180301/>)

### Acknowledgements

This work made use of data from the FAST. FAST is a Chinese national megascience facility, built and operated by the National Astronomical Observatories, Chinese Academy of Sciences. This work is supported by National SKA Program of China (2020SKA0120100, 2020SKA0120200), Natural Science Foundation of China (12041304, 11873067, 11988101, 12041303, 11725313, 11725314, 11833003, 12003028, 12041306, 12103089, U2031209, U2038105, U1831207), KJL acknowledges funding from the Max-Planck Partner Group and support from the XPLOER PRIZE.

### Author Contributions

JCJ and JWX led the data analysis of polarization and drafted the manuscript, JRN worked on the PA jump, KJL, WWZ, and BZ coordinated the observational campaign, cosupervised data analyses and interpretations, and led the paper writing. HX, DJZ, YKZ, BJW, SC and CFZ contributed to radio data analysis. YPM contributed to the searching software development. HQG, JLH, HL, LQ, JHS, RY, YLY, DJY, and

YZ aided with FAST observations and coordination. KJL, BZ, YQ, SSC, WYW, DZL, RXX, WL, YPY YL, and RL provided theoretical discussions. LFH, YXH, ZXL, and YHX tested searching software, and coordinated S-band observation.

### Competing Interests

The authors declare no competing financial interests.

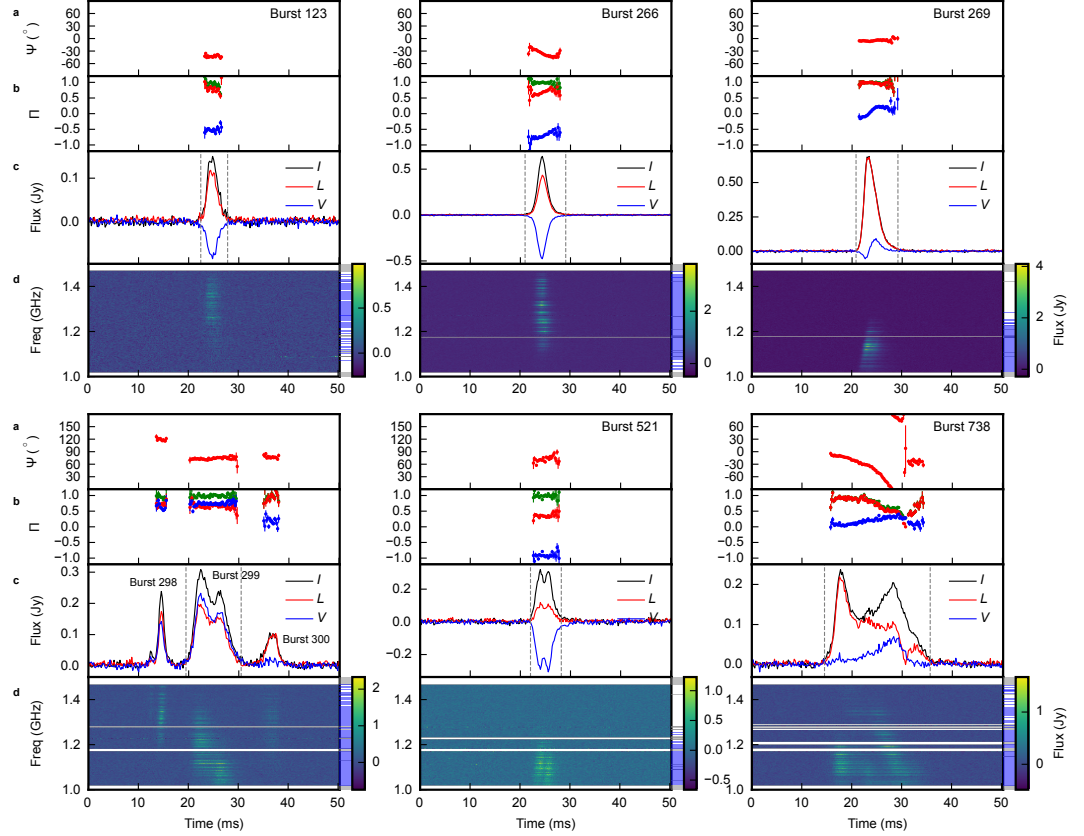


Figure 1: Polarimetric results of a selected sample of bursts with high degrees of circular polarization or abrupt jumps in linear polarization polarization angle. For each burst, we plot **a**) position angle, **b**) degree of linear (red), circular (blue) and total polarization (green) as a function of burst time, **c**) burst profile of total intensity (black), linearly polarization (red), and circular polarization (blue), and **d**) dynamic spectra of the bursts, i.e. intensity as function of time and frequency. The grey shades denote the removed frequency channels affected by RFI and the 20 MHz band edges, and the blue shades denote the frequency channels where the burst signal appears. Here, the frequency resolution of spectra is 1.95 MHz per channel, and the time resolution of the light curves and spectra is 196  $\mu$ s per sample. Errorbars are for 68% confidence level. Bursts are de-dispersed with the daily average DM value published previously [32], which are 412.5  $\text{pc cm}^{-3}$  for Bursts 123, 266 and 269, and 411.6  $\text{pc cm}^{-3}$  for other bursts in this figure. Bursts 298, 299 and 300 are plotted in the same panel as they are very close in time.

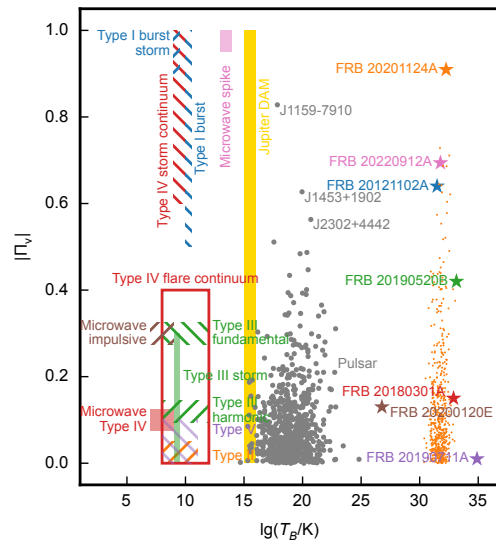


Figure 2: Astrophysical sources with significant circular polarization in the radio band. The x-axis is the brightness temperature. The y-axis is the degree of circular polarization  $\Pi_v$ . For FRBs, the maximal reported  $\Pi_v$  is plotted with star symbols. All the bursts with  $S/N \geq 50$  of FRB 20201124A are also included (orange dots) for reader's reference. The details of the data sources are presented in Section S5 of the online Supplementary Data.

# Supplementary data for Ninety percent circular polarization detected in a repeating fast radio burst

## Radio observations and burst detection

FAST observed FRB 20201124A between September 25 and October 17, 2021 [17,32–34]. In total, we have 19 hours of observations. Bursts were only detected between September 25 and 28. We pointed the central beam of the 19-beam receiver of FAST [51] to the coordinate provided by EVN, RA = 05<sup>h</sup>08<sup>m</sup>03.5077<sup>s</sup>, Dec = +26°03′38.504″ [52]. The 19-beam receiver covers the frequency range of 1 – 1.5 GHz. Search-mode filterbank data with four Stokes parameters were recorded for polarimetry studies using the pulsar digital backend [51,53] in PSRFITS format [49]. The full band, i.e. 1 to 1.5 GHz, was divided into 4096 frequency channels, and we record data at the temporal resolution of 49.152  $\mu$ s per sample.

We follow the rather standard procedures [13,14] to search for burst signals using the software package *TransientX* [54,55]. The software can be found in the ‘Code Availability’ section. The dispersion delay in cold plasma of free electrons is,

$$\Delta t = \mathcal{D} \frac{DM}{\nu^2}, \quad (1)$$

where DM is dispersion measure,  $\nu$  is frequency, and constant  $\mathcal{D} = 4.148808 \times 10^3 \text{ MHz}^2 \text{ pc}^{-1} \text{ cm}^3 \text{ s}$ . Pulses were de-dispersed with the daily average DM value published previously [32], which are 412.4, 412.2, 412.5 and 411.6  $\text{pc cm}^{-3}$  for the 4 days from the 25th to the 28th September, respectively. Then, the burst signals were searched using boxcar matched filters with widths ranging from 0.1 to 100 ms with the signal-to-noise ratio threshold of 7. RFIs were mitigated in the search. The continuous narrow band satellite RFIs are removed according to the RFI list, and a zero-DM matched filter is used to identify wideband RFIs without dispersion [54]. The searching results were later verified by human inspection so that the collected bursts are with a clear dispersive signature. Once the bursts were detected, we further removed data in the 20 MHz band edges at both lower and upper frequency ends for our later analysis.

## Polarization calibration

The 19-beam receiver of FAST uses orthogonal dual linear polarization feeds to receive radio signals [51]. In the first and the last minutes of the observation, modulated signals from a noise diode were injected as a 45° linearly polarized calibrator. The period of modulated noise signals was 100.663296 ms and their duty cycle was 50%. We used software package *DSPSR* [56] to fold the modulated noise signals, and then used software package *PSRCHIVE* [49,57] to calibrate polarization data with the single-axial model. After the polarimetric calibration, the systematical error is at the level of 0.5% [13,14,58]. In this manuscript, we adopt the PSR/IEEE convention [50] for the definitions of the Stokes parameters. We checked and found that the polarization properties are essentially not affected by the DM values we use. For most bursts, the polarization profiles using daily averaged DM or DM from maximizing the structure show no visual differences. Most of the bursts that show large differences are due to their complex structures in the dynamic spectra, for which DM inference is unstable. In this paper, we show the polarisation measurements with daily averaged DM.

## Measurement and Correction of Faraday Rotation

Linear polarization is rotated with frequency, when radio waves propagate through a magnetized plasma. The change of the position angle is,

$$\Delta \text{PA} = \text{RM} \lambda^2, \quad (2)$$

where  $\lambda$  is the wavelength of the radio wave. Similar to previous work [14], we used the Bayesian method [13,59] to fit the rotation of Stokes  $Q$  and  $U$  as a function of frequencies to derive the rotation

measures (RMs) of the bursts. We also cross checked the results with the revisited rotation measure synthesis method [60]. We had corrected the RM contribution caused by the geomagnetic field and Earth ionosphere using the estimation from the software package `ionFR` [61]. Linearly polarized intensity  $L$ , polarized intensity  $P$  and PA were calculated after correcting Faraday rotation to the infinite frequency. The generalized Weisberg correction [17,62] was applied when calculating  $L$  and  $P$ .

### Flux Density and Burst Energy

Our flux calibration for all the bursts are identical with the previous work. For the details of flux and energy estimation, we refer readers to Ref. [14,17,63]. The flux densities  $S$  were estimated using the radiometer equation,

$$S_\nu = \frac{T_{\text{sys}}(S/N)}{G\sqrt{2B\tau}}, \quad (3)$$

where the system temperature  $T_{\text{sys}} \approx 24$  K, gain  $G \approx 16$  K Jy<sup>-1</sup> [51], and  $B$  and  $\tau$  are the signal bandwidth and burst duration, respectively. The fluences  $F$  are calculated by integrating the flux densities over the pulse duration. We compute the burst fluence using three approaches: 1) we average the detected signal within the 500 MHz observing band and 2) we fit the spectrum of a burst with a Gaussian function, then we estimate the fluence using the fitted Gaussian function. Both methods can be affected by scintillation and the limited observing bandwidth, as the true signal central frequency may lay outside of the observing band. In order to avoid the problem, we also took the third approach by generating a subset of the data with the central frequency inside the observing band. However, the number of bursts in the sample is limited. The distribution of burst fluence is shown in Figure SS2, where we also compare the fluence distributions for the bursts with high and low degrees of circular polarization. We note that the conclusion is not affected by how we compute the fluence.

To check if the fluence distribution of the bursts with high degree circular polarization ( $\Pi_\nu > 50\%$ ) are different comparing to that of the bursts with  $\Pi_\nu \leq 50\%$ , we perform the standard two-sample Kolmogorov-Smirnov test [64] between the fluence distributions. Here, the null hypothesis claims that the fluence distributions of large and small degrees of circular polarization are identical, while the alternative claims that the energy distributions are different. We get a p-value of 0.39 for fluence averaged in the observing band, 0.95 for the the Gaussian fitted spectral peak fluence for all the bursts, and 0.30 for the Gaussian fitted spectral peak fluence for the bursts whose peak frequency falls in the observing band in the Kolmogorov-Smirnov test, which cannot reject the null hypothesis, i.e. we cannot differentiate the energy distributions of the two samples.

To investigate if the null result is caused by the limited number of samples, we performed simulations to evaluate the statistical power of the Kolmogorov-Smirnov test for the current limited sample of bursts. In our simulation, an fluence factor ( $\leq 1$ ) is multiplied to the fluence of high  $\Pi_\nu$  bursts, and then we perform the Kolmogorov-Smirnov test and compute the p-value. The procedure is carried out for a uniform grid of fluence factor from 0.01 to 1.0. We can thus compute the fluence factors at which the null hypothesis can be rejected for a given confidence level. As shown in Figure SS3, one would claim a 2-sigma detection, i.e. p-value of 0.05, when the energy of high  $\Pi_\nu$  burst drop to approximately 65% for fluence averaged in the observing band, 35% for the Gaussian fitted fluence peak for all the bursts, and 8% for the Gaussian fitted fluence peak for the bursts whose peak falls in the observing band. In this way, our data set is sensitive to 35% energy difference between the high and low  $\Pi_\nu$  bursts, i.e. we would detect the energy difference of the two population, if the high  $\Pi_\nu$  bursts were 35% weaker. Thus, any theoretical model predicting significant correlation between burst energy and  $\Pi_\nu$  would be in tension with our observations.

### Astrophysical sources with significant circular polarization

In Figure 2, we collected the brightness temperature and degree of circular polarization of various astrophysical sources, including solar radio bursts, Jupiter, radio pulsars, and FRBs. Our data source for solar radio bursts are from Ref. [65]. For radio emission from Jupiter and its magnetosphere, there are three possibilities [66]: i) thermal emission from planetary disks, ii) auroral cyclotron emission below 40 MHz, including decimeter (DAM), hectometer (HOM) and broadband kilometer (bKOM) emissions, iii) synchrotron emission between 30 MHz and 30 GHz. Because we focus on the burst-

like sources, we only include the Jovian DAM emission in Figure 2. The brightness temperature of Jovian DAM can reach  $> 10^{15}$  K [67], while the degree of circular polarization of some bursts approach 100% [68].

A fraction of pulsars exhibit strong circular polarization [69]. We include the polarization observation of normal pulsars [70] and millisecond pulsars [71] in Figure 2. We collected the period, flux and pulse width from the ATNF Pulsar Catalogue [72]. The brightness temperature of a pulsar is estimated [73] using  $T_b = SD^2c^2/2kAv^2$ , where  $S$  is the observed radio flux,  $D$  is the pulsar distance.  $A$  is the effective magnetosphere area and estimated using the pulse timescale, i.e.  $A = \pi W^2c^2$ , with  $W$  being the pulse width at half of peak. Constants  $k$  and  $c$  are the Boltzmann constant and light speed, respectively.

For FRBs, non-detection or marginal detection of circular polarization has been previously reported for FRB repeaters, e.g. FRB 20121102A [74–77], FRB 20180301A [78], 20190711A [24], and 20220912A [79]. In addition to FRB 20201124A, circularly polarized emission has been sporadically detected from a few FRB repeaters. Circular polarization has also been reported in bursts from FRB 20220912A [19,30] (70%) and FRB 20190520B [28] (42%). Recently, circular polarization of 64% from FRB 20121102A was also reported [29]. In Figure 2, the highest values of published  $\Pi_v$  are collected. The brightness temperature of FRB is estimated [41] using

$$T_b = \frac{SD_L^2}{2\pi k_B(1+z)v^2\Delta t^2}, \quad (4)$$

where  $D_L$  is the luminosity distance derived from the redshift  $z$ , and, similar to the pulsar case, the burst time width  $\Delta t$  is used to estimate the size of emission zone [41].

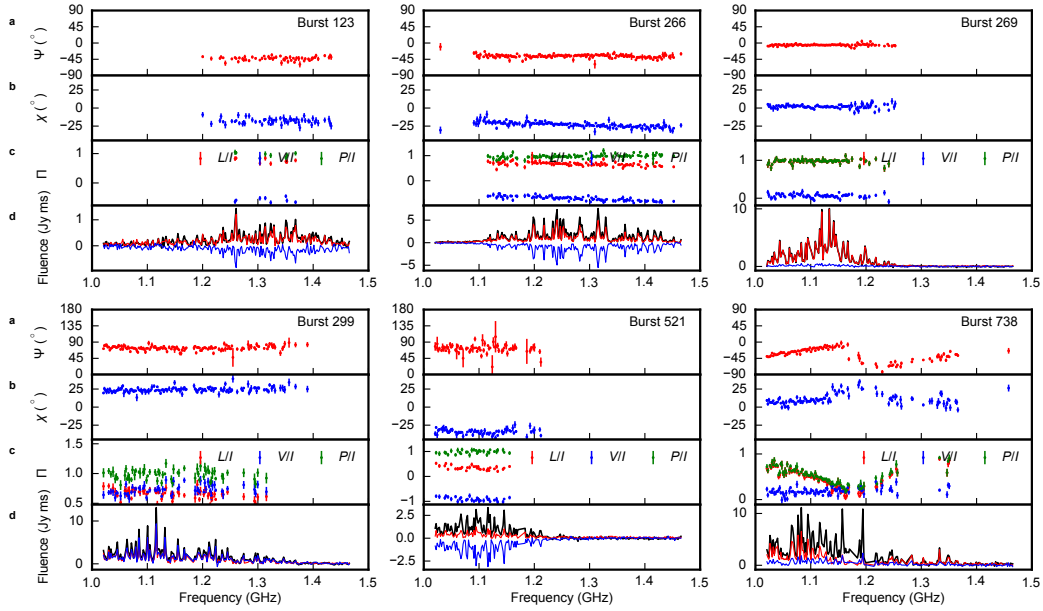


Figure S1: polarization spectra of selected sample of bursts with high degrees of circular polarization or abrupt jumps in linear polarization position angle. For each burst, we plotted **a**) Position angle, **b**) Ellipticity angle, **c**) degree of linear (red), circular (blue) and total polarization (green), and **d**) Burst fluence of total intensity (black), linearly polarization (red), and circular polarization (blue) as functions of frequency.

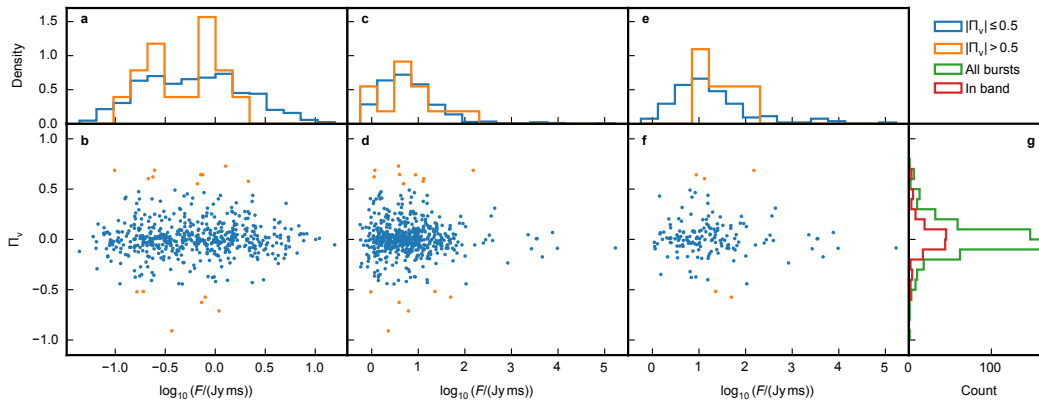


Figure S2: The distribution of burst fluence and degree of circular polarization ( $\Pi_v$ ) for burst with  $S/N \geq 50$ . a) histogram of burst fluence averaged in the observing band, bursts with  $\Pi_v \geq 50\%$  are in orange, while the other bursts are in blue. b) two dimensional distribution of burst fluence averaged in the observing band and  $\Pi_v$  with the same color convention of a). c) histogram of burst fluence using Gaussian fitted spectra for all the bursts. d) two dimensional distribution of fluence using Gaussian fitted spectra and  $\Pi_v$  for all the bursts. e) histogram of burst fluence using Gaussian fitted spectra for the bursts with spectral peak in the observing band. f) two dimensional distribution of fluence using Gaussian fitted spectra and  $\Pi_v$  for the bursts with spectral peak in the observing band. g) Histogram of  $\Pi_v$  for all bursts and bursts with spectral peak in the observing band.



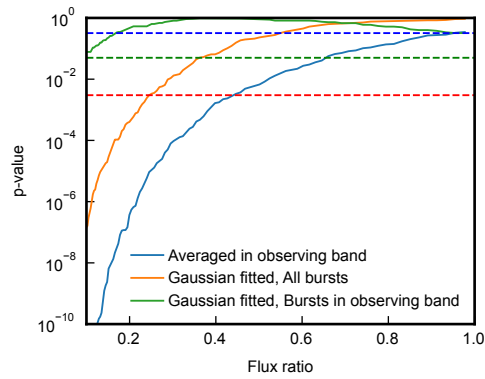


Figure S3: The relation between the p-value of Kolmogorov-Smirnov test and energy factor multiplied to the energy of bursts with  $\Pi_v \geq 50\%$ . The blue curves are the p-value and energy factor relation. The blue, green, and red dashed lines are for 1-, 2-, and 3- $\sigma$ , i.e. p-value of 32%, 5%, and 0.3 %, respectively.

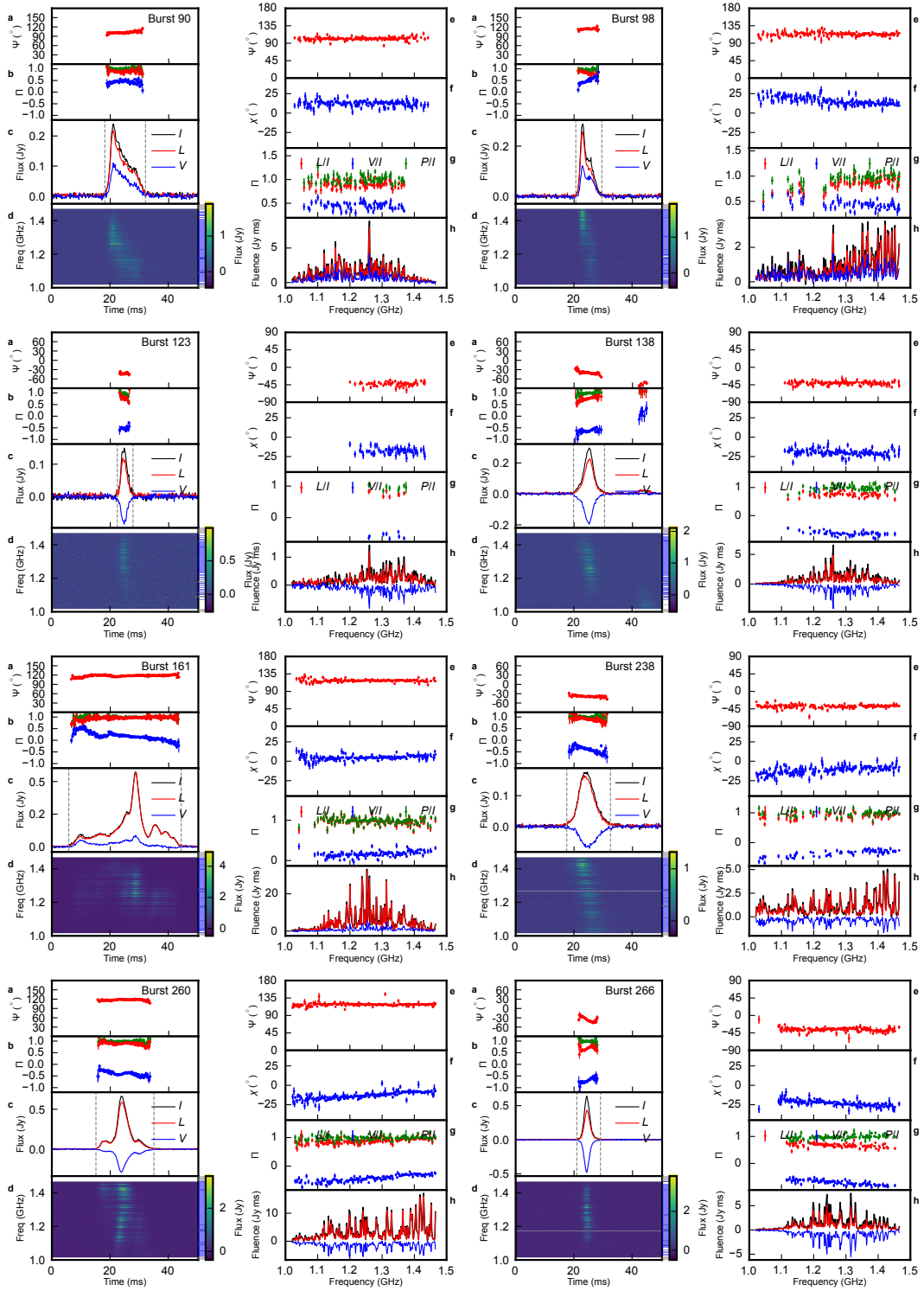


Figure S4: Bursts with  $\Pi_V \geq 50\%$  and  $S/N \geq 50$ . Notations are the same as in Figure 1.

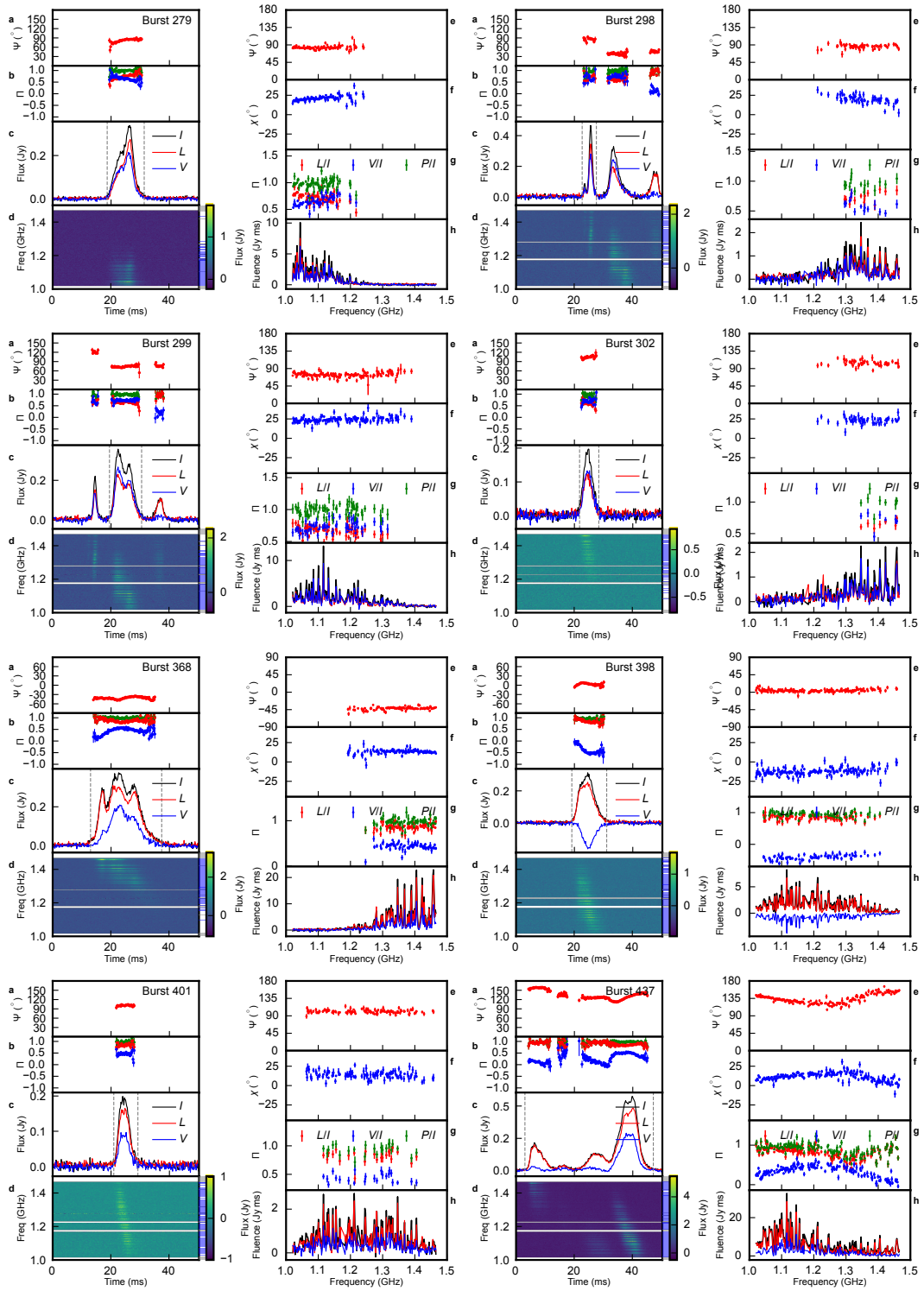


Figure S5: Continuation of Figure SS4.

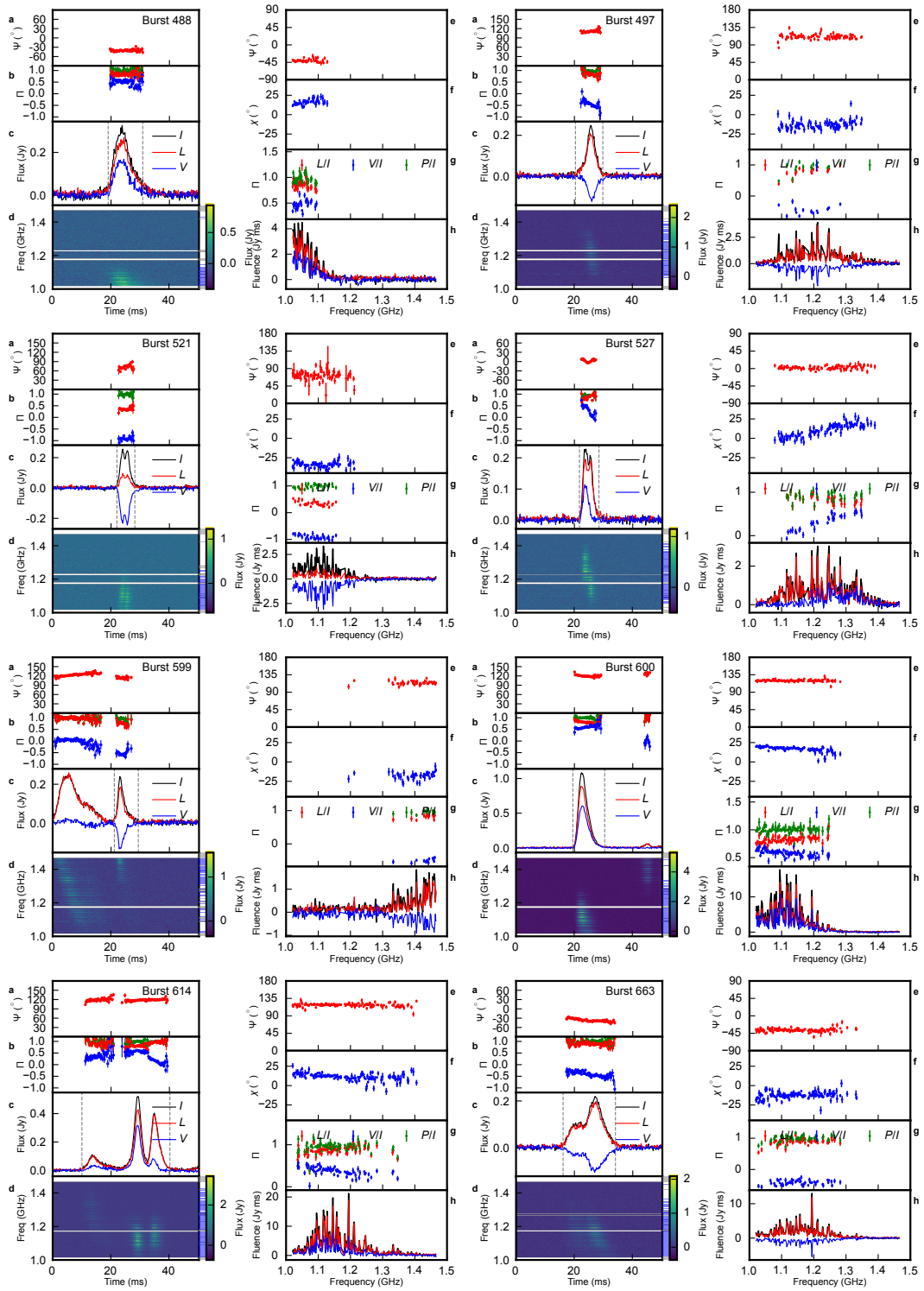


Figure S6: Continuation of Figure SS4.

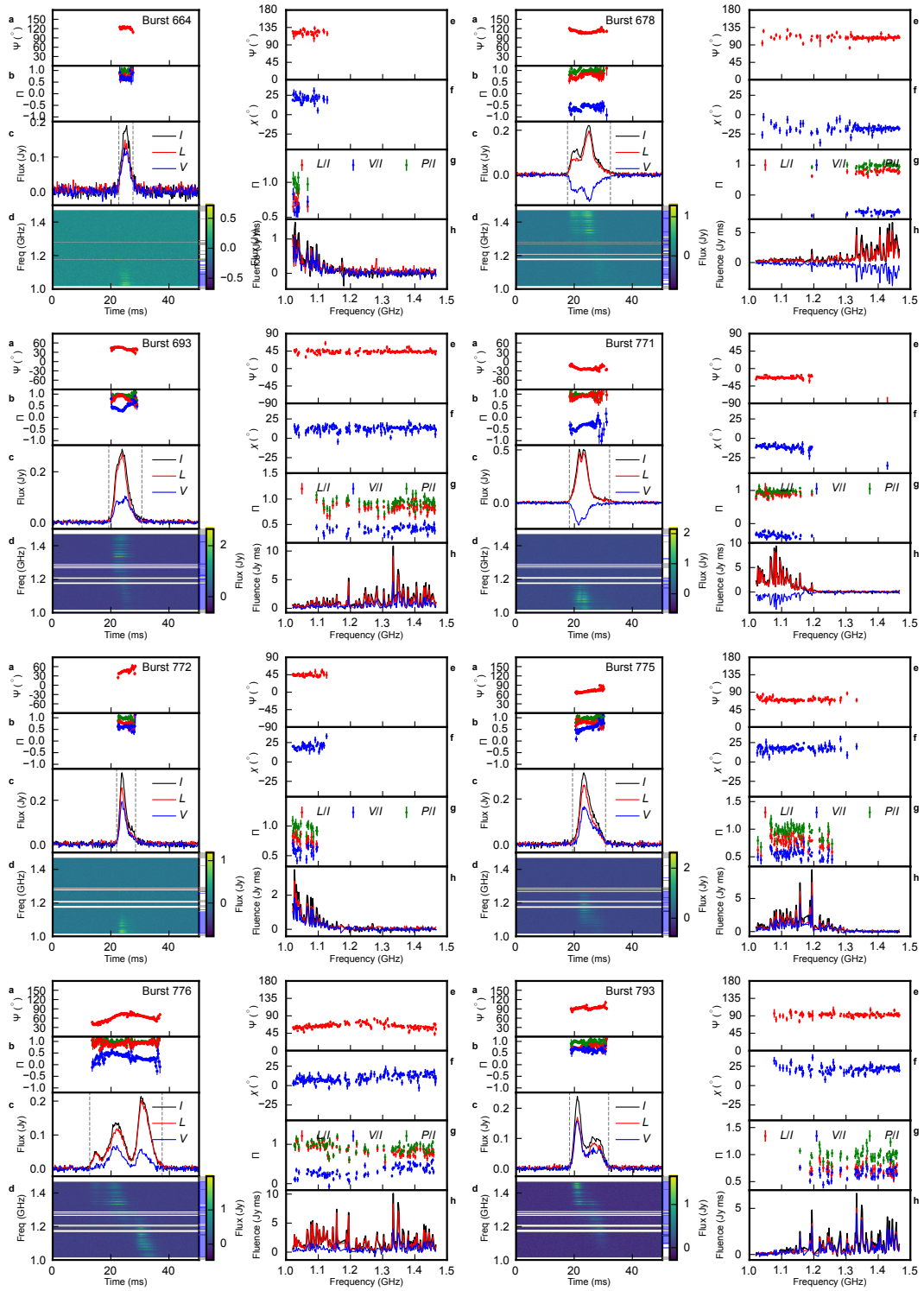


Figure S7: Continuation of Figure SS4.

Table S1: Summary of high  $\Pi_v$  burst properties. Uncertainties are for 68% confidence interval.

No. <sup>a</sup>	TOA <sup>b</sup> day	RM <sub>Bayes</sub> <sup>c</sup> rad m <sup>-2</sup>	(L/I) <sup>d</sup> %	(V/I) <sub>mean</sub> <sup>e</sup> %	(V/I) <sub>peak</sub> <sup>f</sup> %	P/I <sup>g</sup> %	Peak flux Jy	Fluence <sup>h</sup> Jy ms
90	0.818177	-584.9 ± 0.5	88.3 ± 0.7	43.7 ± 0.5	56.5 ± 3.5	98.5 ± 0.7	0.51	1.5
98	0.819599	-591.7 ± 0.5	82.2 ± 0.7	46.5 ± 0.6	61 ± 5	94.4 ± 0.8	0.66	1.0
123	0.825277	-578.9 ± 2.3	75.6 ± 1.7	-52.1 ± 1.6	-57 ± 5	91.8 ± 1.9	0.35	0.4
138	0.828698	-583.5 ± 0.8	75.0 ± 0.7	-62.6 ± 0.6	-68.8 ± 2.3	97.7 ± 0.7	0.69	1.2
161	0.833527	-594.23 ± 0.28	96.34 ± 0.26	16.38 ± 0.19	58 ± 5	97.72 ± 0.26	1.40	5.3
238	0.845965	-590.38 ± 0.35	91.4 ± 0.7	-37.8 ± 0.5	-56 ± 4	99.0 ± 0.7	0.47	1.2
260	0.849867	-593.39 ± 0.2	89.50 ± 0.24	-40.12 ± 0.19	-58.3 ± 3.5	98.08 ± 0.25	1.76	3.5
266	0.851199	-595.6 ± 0.6	66.86 ± 0.35	-71.1 ± 0.4	-80.3 ± 3.5	97.6 ± 0.4	1.70	1.5
279	0.853596	-594.2 ± 0.7	73.0 ± 0.5	64.2 ± 0.5	83 ± 4	97.3 ± 0.6	0.90	1.9
298	1.786479	-585.3 <sup>+2.7</sup> <sub>-3.0</sub>	71.2 ± 1.5	62.1 ± 1.4	72.6 ± 3.2	94.5 ± 1.7	0.73	0.7
299	1.786479	-596.2 ± 0.7	65.6 ± 0.6	72.9 ± 0.6	78.8 ± 2.9	98.0 ± 0.7	0.50	2.1
302	1.786862	-612.6 ± 3.4	61.1 ± 1.6	68.7 ± 1.7	-	91.9 ± 1.8	0.32	0.7
368	1.792096	-622.1 ± 0.7	87.0 ± 0.4	43.79 ± 0.34	59.7 ± 3.3	97.4 ± 0.4	0.66	4.8
398	1.794975	-613.0 ± 0.4	84.3 ± 0.6	-40.7 ± 0.5	-58.1 ± 2.6	93.6 ± 0.7	0.48	1.8
401	1.795033	-621.0 ± 0.8	83.3 ± 1.2	45.2 ± 1.0	54 ± 4	94.8 ± 1.3	0.32	0.9
437	1.797915	-637.9 ± 1.2	79.52 ± 0.32	35.83 ± 0.27	54.9 ± 1.2	87.21 ± 0.33	0.85	6.2
488	1.802788	-588.4 <sup>+2.1</sup> <sub>-2.0</sub>	82.4 ± 1.1	49.0 ± 1.0	59 ± 5	95.9 ± 1.2	3.62	2.0
497	1.803396	-579.7 ± 1.3	81.8 ± 1.3	-43.9 ± 1.1	-55 ± 4	92.9 ± 1.4	0.42	0.9
521	1.804982	-568.4 <sup>+2.8</sup> <sub>-2.7</sub>	34.3 ± 0.9	-90.9 ± 1.1	-100 ± 4	97.2 ± 1.2	0.52	1.1
527	1.805791	-615.4 ± 0.9	84.3 ± 1.1	30.7 ± 0.9	52.4 ± 3.3	89.7 ± 1.1	0.41	0.8
599	1.810067	-610.8 <sup>+3.3</sup> <sub>-3.5</sub>	74.0 ± 1.7	-51.7 ± 1.6	-61 ± 4	90.3 ± 1.9	0.51	0.7
600	1.810074	-613.0 ± 0.4	81.07 ± 0.28	57.80 ± 0.25	69.8 ± 2.4	99.56 ± 0.30	1.90	4.2
614	1.810844	-619.3 ± 0.5	87.7 ± 0.5	37.8 ± 0.4	62.2 ± 1.3	95.5 ± 0.5	0.92	3.6
663	1.814971	-595.3 ± 0.7	88.3 ± 0.7	-41.8 ± 0.6	-55 ± 4	97.7 ± 0.8	0.42	1.9
664	1.815084	-612.2 <sup>+3.4</sup> <sub>-3.5</sub>	74.3 ± 2.2	68.6 ± 2.1	-	101.1 ± 2.5	0.36	0.6
678	1.815578	-614.2 ± 1.0	78.2 ± 0.8	-57.4 ± 0.7	-59.8 ± 3.2	97.0 ± 0.9	0.50	1.3
693	1.817261	-594.9 ± 0.4	83.6 ± 0.6	40.3 ± 0.5	58.4 ± 3.3	92.8 ± 0.6	0.64	1.4
771	1.823548	-597.3 ± 0.8	89.6 ± 0.6	-37.0 ± 0.4	-60.5 ± 3.1	97.0 ± 0.6	1.08	2.5
772	1.823569	-583.8 <sup>+1.8</sup> <sub>-1.7</sub>	75.4 ± 1.2	60.4 ± 1.1	66 ± 4	96.6 ± 1.3	0.70	0.9
775	1.823892	-604.8 ± 0.7	78.4 ± 0.7	55.3 ± 0.6	62 ± 4	96.0 ± 0.7	0.67	1.5
776	1.824116	-613.0 ± 0.5	87.6 ± 0.6	31.7 ± 0.5	54 ± 4	93.2 ± 0.6	0.46	2.0
793	1.824974	-594.8 ± 0.7	71.9 ± 0.7	64.5 ± 0.7	74 ± 4	96.6 ± 0.8	0.60	1.3

<sup>a</sup> Burst index number.<sup>b</sup> Barycentric burst time of arrival in Barycentric Coordinate Time (TCB) scale. The time reference of  $T = 0$  is MJD 59484.<sup>c</sup> Faraday rotation measure using Bayesian method after correcting the Earth ionosphere contribution.<sup>d</sup> Average degree of linear polarization.<sup>e</sup> Average degree of circular polarization.<sup>f</sup> Peak degree of circular polarization.<sup>g</sup> Average degree of total polarization.<sup>h</sup> Average fluence in the burst frequency channels.

## REFERENCES

- Bochenek CD, Ravi V, Belov KV *et al.* A fast radio burst associated with a Galactic magnetar. *Nature* 2020; **587**: 59–62.
- CHIME/FRB Collaboration, Andersen BC, Bandura KM *et al.* A bright millisecond-duration radio burst from a Galactic magnetar. *Nature* 2020; **587**: 54–58.
- Zhang B. The physical mechanisms of fast radio bursts. *Nature* 2020; **587**: 45–53.
- Metzger BD, Margalit B and Sironi L. Fast radio bursts as synchrotron maser emission from decelerating relativistic blast waves. *Monthly Notices of the Royal Astronomical Society* 2019; **485**: 4091–4106.
- Beloborodov AM. Blast Waves from Magnetar Flares and Fast Radio Bursts. *Astrophysical Journal Supplement Series* 2020; **896**:142.
- Kumar P, Lu W and Bhattacharya M. Fast radio burst source properties and curvature radiation model. *Monthly Notices of the Royal Astronomical Society* 2017; **468**: 2726–2739.
- Yang YP and Zhang B. Bunching Coherent Curvature Radiation in Three-dimensional Magnetic Field Geometry: Application to Pulsars and Fast Radio Bursts. *Astrophysical Journal Supplement Series* 2018; **868**:31.
- Wang WY, Yang YP, Niu CH *et al.* Magnetospheric Curvature Radiation by Bunches as Emission Mechanism for Repeating Fast Radio Bursts. *Astrophysical Journal* 2022; **927**:105.
- Wang WY, Jiang JC, Lu J *et al.* Repeating fast radio bursts: Coherent circular polarization by bunches. *Science China Physics, Mechanics, and Astronomy* 2022; **65**:289511.
- Zhang B. Coherent Inverse Compton Scattering by Bunches in Fast Radio Bursts. *Astrophysical Journal* 2022; **925**:53.
- Qu Y and Zhang B. Polarization of fast radio bursts: radiation mechanisms and propagation effects. *Monthly Notices of the Royal Astronomical Society* 2023; **522**: 2448–2477.
- Price DC, Foster G, Geyer M *et al.* A fast radio burst with frequency-dependent polarization detected during Breakthrough Listen observations. *MNRAS* 2019; **486**: 3636–3646.
- Luo R, Wang BJ, Men YP *et al.* Diverse polarization angle swings from a repeating fast radio burst source. *Nature* 2020; **586**: 693–696.
- Xu H, Niu JR, Chen P *et al.* A fast radio burst source at a complex magnetized site in a barred galaxy. *Nature* 2022; **609**: 685–688.

15. Hilmarsson GH, Spitler LG, Main RA et al. Polarization properties of FRB 20201124A from detections with the Effelsberg 100-m radio telescope. Monthly Notices of the Royal Astronomical Society 2021; **508**: 5354–5361.
16. Kumar P, Shannon RM, Lower ME et al. Circularly polarized radio emission from the repeating fast radio burst source FRB 20201124A. Monthly Notices of the Royal Astronomical Society 2022; .
17. Jiang JC, Wang WY, Xu H et al. FAST Observations of an Extremely Active Episode of FRB 20201124A. III. Polarimetry. Research in Astronomy and Astrophysics 2022; **22**:124003.
18. Kumar P, Shannon RM, Lower ME et al. Propagation of a fast radio burst through a birefringent relativistic plasma. Physical Review D 2023; **108**:043009.
19. Feng Y, Li D, Zhang YK et al. An extreme active repeating fast radio burst in a clean environment. arXiv e-prints 2023; arXiv:2304.14671.
20. Masui K, Lin HH, Sievers J et al. Dense magnetized plasma associated with a fast radio burst. Nature 2015; **528**: 523–525.
21. Petroff E, Bailes M, Barr ED et al. A real-time fast radio burst: polarization detection and multiwavelength follow-up. Monthly Notices of the Royal Astronomical Society 2015; **447**: 246–255.
22. Caleb M, Keane EF, van Straten W et al. The SUrvey for Pulsars and Extragalactic Radio Bursts - III. Polarization properties of FRBs 160102 and 151230. Monthly Notices of the Royal Astronomical Society 2018; **478**: 2046–2055.
23. Osłowski S, Shannon RM, Ravi V et al. Commensal discovery of four fast radio bursts during Parkes Pulsar Timing Array observations. Monthly Notices of the Royal Astronomical Society 2019; **488**: 868–875.
24. Day CK, Deller AT, Shannon RM et al. High time resolution and polarization properties of ASKAP-localized fast radio bursts. Monthly Notices of the Royal Astronomical Society 2020; **497**: 3335–3350.
25. Prochaska JX, Macquart JP, McQuinn M et al. The low density and magnetization of a massive galaxy halo exposed by a fast radio burst. Science 2019; **366**: 231–234.
26. Cho H, Macquart JP, Shannon RM et al. Spectropolarimetric Analysis of FRB 181112 at Microsecond Resolution: Implications for Fast Radio Burst Emission Mechanism. Astrophysical Journal Letters 2020; **891**:L38.
27. Mckinven R, Michilli D, Masui K et al. Polarization Pipeline for Fast Radio Bursts Detected by CHIME/FRB. Astrophysical Journal Supplement Series 2021; **920**:138.
28. Anna-Thomas R, Connor L, Dai S et al. Magnetic field reversal in the turbulent environment around a repeating fast radio burst. Science 2023; **380**: 599–603.
29. Feng Y, Zhang YK, Li D et al. Circular polarization in two active repeating fast radio bursts. Science Bulletin 2022; **67**: 2398–2401.
30. Zhang YK, Li D, Zhang B et al. FAST Observations of FRB 20220912A: Burst Properties and Polarization Characteristics. Astrophysical Journal Supplement Series 2023; **955**:142.
31. Ravi V, Catha M, Chen G et al. Deep Synoptic Array Science: Discovery of the Host Galaxy of FRB 20220912A. Astrophysical Journal Letters 2023; **949**:L3.
32. Zhou DJ, Han JL, Zhang B et al. FAST Observations of an Extremely Active Episode of FRB 20201124A: I. Burst Morphology. Research in Astronomy and Astrophysics 2022; **22**:124001.
33. Zhang YK, Wang P, Feng Y et al. FAST Observations of an Extremely Active Episode of FRB 20201124A. II. Energy Distribution. Research in Astronomy and Astrophysics 2022; **22**:124002.
34. Niu JR, Zhu WW, Zhang B et al. FAST Observations of an Extremely Active Episode of FRB 20201124A. IV. Spin Period Search. Research in Astronomy and Astrophysics 2022; **22**:124004.
35. Amiri M, Andersen BC, Bandura K et al. The First CHIME/FRB Fast Radio Burst Catalog. Astrophysical Journal Supplement Series 2021; **257**:59.
36. Wu CS. Kinetic cyclotron and synchrotron maser instabilities: Radio emission processes by direct amplification of radiation. Space Sci. Rev. 1985; **41**: 215–298.
37. Wang C, Lai D and Han J. Polarization changes of pulsars due to wave propagation through magnetospheres. Monthly Notices of the Royal Astronomical Society 2010; **403**: 569–588.
38. Lu JG, Wang WY, Peng B et al. Are pulsar giant pulses induced by re-emission of cyclotron resonance absorption? Research in Astronomy and Astrophysics 2021; **21**:029.
39. Wang FY, Zhang GQ, Dai ZG et al. Repeating fast radio burst 20201124A originates from a magnetar/Be star binary. Nature Communications 2022; **13**:4382.
40. Dai S, Lu J, Wang C et al. On the Circular Polarization of Repeating Fast Radio Bursts. Astrophysical Journal 2021; **920**:46.
41. Zhang B. The physics of fast radio bursts. Reviews of Modern Physics 2023; **95**:035005.
42. Qiao GJ and Lin WP. An inverse Compton scattering (ICS) model of pulsar emission. I. Core and conal emission beams. Astronomy & Astrophysics 1998; **333**: 172–180.
43. Xu RX, Liu JF, Han JL et al. An Inverse Compton Scattering Model of Pulsar Emission. III. Polarization. Astrophysical Journal Supplement Series 2000; **535**: 354–364.
44. Stinebring DR, Cordes JM, Rankin JM et al. Pulsar polarization fluctuations. I. 1404 MHz statistical summaries. Astrophysical Journal Supplement Series 1984; **55**: 247–277.
45. Singh S, Gupta Y and De K. Single pulse polarization study of pulsars B0950 + 08 and B1642 - 03: micropulse properties and mixing of orthogonal modes. Monthly Notices of the Royal Astronomical Society 2024; **527**: 2612–2623.
46. Dyks J. The origin of radio pulsar polarization. Monthly Notices of the Royal Astronomical Society 2017; **472**: 4598–4617.
47. Feng Y, Li D, Yang YP et al. Frequency-dependent polarization of repeating fast radio bursts—implications for their origin. Science 2022; **375**: 1266–1270.



48. Men Y and Barr E. TransientX: A high-performance single-pulse search package. *Astronomy & Astrophysics* 2024; **683**:A183.
49. Hotan AW, van Straten W and Manchester RN. PSRCRIVE and PSRFITS: An Open Approach to Radio Pulsar Data Storage and Analysis. *Publications of the Astronomical Society of Australia* 2004; **21**: 302–309.
50. van Straten W, Manchester RN, Johnston S *et al.* PSRCRIVE and PSRFITS: Definition of the Stokes Parameters and Instrumental Basis Conventions. *Publications of the Astronomical Society of Australia* 2010; **27**: 104–119.
51. Jiang P, Tang NY, Hou LG *et al.* The fundamental performance of FAST with 19-beam receiver at L band. *Research in Astronomy and Astrophysics* 2020; **20**:064.
52. Marcote B, Kirsten F, Hessels JWT *et al.* VLBI localization of FRB 20201124A and absence of persistent emission on milliarc-second scales. *The Astronomer's Telegram* 2021; **14603**: 1.
53. Jiang P, Yue Y, Gan H *et al.* Commissioning progress of the FAST. *Science China Physics, Mechanics, and Astronomy* 2019; **62**:959502.
54. Men YP, Luo R, Chen MZ *et al.* Piggyback search for fast radio bursts using Nanshan 26 m and Kunming 40 m radio telescopes - I. Observing and data analysis systems, discovery of a mysterious peryton. *Monthly Notices of the Royal Astronomical Society* 2019; **488**: 3957–3971.
55. Men Y and Barr E. TransientX: A high performance single pulse search package. *arXiv e-prints* 2024; arXiv:2401.13834.
56. van Straten W and Bailes M. DSPSR: Digital Signal Processing Software for Pulsar Astronomy. *Publications of the Astronomical Society of Australia* 2011; **28**: 1–14.
57. van Straten W, Demorest P and Oslowski S. Pulsar Data Analysis with PSRCRIVE. *Astronomical Research and Technology* 2012; **9**: 237–256.
58. Dunning A, Bowen M, Castillo S *et al.* Design and laboratory testing of the five hundred meter aperture spherical telescope (fast) 19 beam I-band receiver. *XXXIInd General Assembly and Scientific Symposium of the International Union of Radio Science* (2017) 1–4.
59. Desvignes G, Kramer M, Lee K *et al.* Radio emission from a pulsar's magnetic pole revealed by general relativity. *Science* 2019; **365**: 1013–1017.
60. Schnitzeler DHFM and Lee KJ. Rotation measure synthesis revisited. *Monthly Notices of the Royal Astronomical Society* 2015; **447**: L26–L30.
61. Sotomayor-Beltran C, Sobey C, Hessels JWT *et al.* Calibrating high-precision Faraday rotation measurements for LOFAR and the next generation of low-frequency radio telescopes. *Astronomy & Astrophysics* 2013; **552**:A58.
62. Everett JE and Weisberg JM. Emission Beam Geometry of Selected Pulsars Derived from Average Pulse Polarization Data. *Astrophysical Journal Supplement Series* 2001; **553**: 341–357.
63. Chime/Frb Collaboration, Amiri M, Andersen BC *et al.* Periodic activity from a fast radio burst source. *Nature* 2020; **582**: 351–355.
64. Press W, Teukolsky S, Vetterling WT *et al.* *Numerical Recipes 3rd Edition: The Art of Scientific Computing* (Cambridge University Press, New York, NY, USA), 3 edition.
65. Dulk GA. Radio emission from the sun and stars. *Annual Review of Astronomy and Astrophysics* 1985; **23**: 169–224.
66. Girard JN, Zarka P, Tasse C *et al.* Imaging Jupiter's radiation belts down to 127 MHz with LOFAR. *Astronomy & Astrophysics* 2016; **587**:A3.
67. Clarke TE, Higgins CA, Skarda J *et al.* Probing Jovian decametric emission with the long wavelength array station 1. *Journal of Geophysical Research (Space Physics)* 2014; **119**: 9508–9526.
68. Marques MS, Zarka P, Echer E *et al.* Statistical analysis of 26 yr of observations of decametric radio emissions from Jupiter. *Astronomy & Astrophysics* 2017; **604**:A17.
69. Han JL, Manchester RN, Xu RX *et al.* Circular polarization in pulsar integrated profiles. *Monthly Notices of the Royal Astronomical Society* 1998; **300**: 373–387.
70. Johnston S and Kerr M. Polarimetry of 600 pulsars from observations at 1.4 GHz with the Parkes radio telescope. *Monthly Notices of the Royal Astronomical Society* 2018; **474**: 4629–4636.
71. Spiewak R, Bailes M, Miles MT *et al.* The MeerTime Pulsar Timing Array: A census of emission properties and timing potential. *Publications of the Astronomical Society of Australia* 2022; **39**:e027.
72. Manchester RN, Hobbs GB, Teoh A *et al.* The Australia Telescope National Facility Pulsar Catalogue. *Astronomical Journal* 2005; **129**: 1993–2006.
73. Lorimer DR and Kramer M. *Handbook of Pulsar Astronomy* (Cambridge University Press, New York, NY, USA).
74. Michilli D, Seymour A, Hessels JWT *et al.* An extreme magneto-ionic environment associated with the fast radio burst source FRB 121102. *Nature* 2018; **553**: 182–185.
75. Gajjar V, Siemion APV, Price DC *et al.* Highest Frequency Detection of FRB 121102 at 4–8 GHz Using the Breakthrough Listen Digital Backend at the Green Bank Telescope. *Astrophysical Journal Supplement Series* 2018; **863**:2.
76. Faber JT, Gajjar V, Siemion APV *et al.* Re-analysis of Breakthrough Listen Observations of FRB 121102: Polarization Properties of Eight New Spectrally Narrow Bursts. *Research Notes of the American Astronomical Society* 2021; **5**:17.
77. Hilmarsson GH, Michilli D, Spitler LG *et al.* Rotation Measure Evolution of the Repeating Fast Radio Burst Source FRB 121102. *Astrophysical Journal Letters* 2021; **908**:L10.
78. Kumar P, Luo R, Price DC *et al.* Spectropolarimetric variability in the repeating fast radio burst source FRB 20180301A. *Monthly Notices of the Royal Astronomical Society* 2023; **526**: 3652–3672.
79. Hewitt DM, Hessels JWT, Ould-Boukattine OS *et al.* Dense forests of microshots in bursts from FRB 20220912A. *Monthly Notices of the Royal Astronomical Society* 2023; **526**: 2039–2057.